Growth of Robust Carbon Nitride Films by Double Inoculation with Exceptionally Boosted Electrochemiluminescence

Yuhua Hou,‡ Yanfeng Fang,‡ Zhixin Zhou, Qing Hong, Wang Li, Hong Yang, Kaiqing Wu, Yuan Xu, Xuwen Cao, Dan Han, Songqin Liu, Yanfei Shen, and Yuanjian Zhang*

Jiangsu Engineering Laboratory of Smart Carbon-Rich Materials and Devices, Jiangsu Province Hi-Tech Key Laboratory for Bio-Medical Research, State Key Laboratory of Bioelectronics, School of Chemistry and Chemical Engineering, Medical School, Southeast University, Nanjing 211189, China.

E-mail: Yuanjian.Zhang@seu.edu.cn

Abstract

Electrochemically generated chemiluminescence (ECL) has attracted significant interest over decades, ranging from fundamental studies of highly efficient electron-to-photon interconversion to practical bioassays. Nonetheless, the ECL efficiency of most emitters is low, which greatly hampers further development. Herein, we report a highly robust carbon nitride film with an unusually boosted ECL efficiency (2256 times higher than that of the reference $Ru(bpy)_3Cl_2/K_2S_2O_8$. Double inoculation, which provided the primary interaction of carbon nitride with the substrate and the succedent growth, played a crucial role in preparation. The improved ECL efficiency was ascribed to few pinholes suppressing futile co-reagent reduction, maintenance of more orbit-delocalized heptazine subunit improving ECL kinetics, and transparency avoiding self-absorption. As a result of the exceptionally high ECL efficiency, an ultrasensitive visual DNA biosensor by the naked eye was further successfully developed.

Keyword: Electrochemiluminescence efficiency; Carbon nitrides; Mechanical properties; Transparency; Visual DNA biosensor

Introduction

The highly efficient interconversion of energy in different forms plays a crucial role not only in living but also in artificial devices. Among them, electrochemiluminescence (ECL), a well-known light emission process whereby excited species are generated at electrode surfaces by electrochemical reactions, has attracted significant interest for decades, ranging from fundamental studies of electron-to-photon conversion to practical applications, particularly in clinical bioassays.[1] Nonetheless, the ECL of most emitters in aqueous solutions, including standard tris(2,2'-bipyridine)ruthenium(II) chloride ($Ru(bpy)_3Cl_2$) and luminol, is essentially low, which greatly hampers further development for highly demanding applications, such as visual ECL analysis that requires sufficient light intensity to be visible to the naked eye.[2] Along this line, great efforts have been devoted to improve the ECL efficiency by strengthening intermolecular charger transfer,[3] radical stabilization,[4] and aggregation effects.[5] Alternatively, several new ECL emitters, such as quantum dots,[6] noble metal clusters, [7] polymer dots,[3a, 8] and metal-organic frameworks, [9] have been proposed. Despite unprecedented success, however, compared with the highly developed similar photoexcitation process, that is, photoluminescence, research on pursuing ECL emitters with high efficiency is still in its infancy. [10] Moreover, for large-scale clinical bioassays, the new ECL emitters still should be low-cost, non-toxic, and environmentally friendly, but this still remains challenging.[1d, 1g, 5a, 11]

Recently, substantial efforts have been devoted to metal-free polymeric carbon nitride (pCN), which has been extensively explored for solar fuels and photoredox reactions.[12] Intriguingly, pCN was also discovered as a new generation of ECL luminophores with record-level cathodic ECL efficiency, owing to its rigid covalently bonded 2D structure and unique photophysical properties.[13] Nonetheless, because of the poor solubility of pCN in most solvents, high-quality, uniform, and tightly packed pCN electrodes, the core of photoelectric interconversion, are difficult to be prepared by common solvent-based methods, such as spray-coating,[14] drop-casting,[15] spin-coating,[16] and inkjet printing.[17] Even by using well-dispersed nanosheets, the grain boundary effects could hardly be avoided in the final pCN film, leading to a high charge-transfer resistance and subsequently significantly suppressed ECL efficiency. [18] In principle, the direct *in situ* growth of a pCN film on a substrate electrode with improved adhesion could bypass the grain boundary and allow better carrier migration.[19] For this purpose, pioneering works, such as thermal vapor condensation, [20] seed crystallization-condensation,[21] template-confined condensation,[22] and ultrafast microwave-assisted condensation,[23] have been successfully developed. Notably, most of these strategies have been used to boost photoelectrochemical performance, focusing on highly efficient light harvesting.[24] In contrast, ECL process emits as much light as possible. Thus, transparent electrodes are preferred to minimize self-absorption. Moreover, ill condensation, which is detrimental to high ECL efficiency, often occurs on substrates owing to unidealized polymerization conditions.[23] Therefore, despite their rapid development, pCN electrodes still exhibit unsatisfactory ECL efficiency.

Herein, we report a facile method to obtain a highly robust and transparent pCN film

(tpCN) on FTO with a new record cathodic ECL efficiency (more than 2000 times higher than that of the reference $Ru(bpy)_3Cl_2/K_2S_2O_8$ system). Direct thermal condensation of the tpCN monomer from double inoculation was used to strengthen the interfacial interaction and minimize the effects of condition differences on tpCN growth. Interestingly, it not only led to intimate contact of the tpCN film with substrate electrodes at the nanoscale level and excellent Young's modules/hardness, but also maintained the same heptazine subunits as the conventional bulk pCN. As a result, compared to previous pCN electrodes, the significantly improved ECL efficiency was observed, because of few pinholes suppressing futile co-reagent reduction, maintenance of more orbit-delocalized heptazine subunit improving ECL kinetics,[25] and transparency avoiding self-absorption. It further enabled the visual ECL detection of DNA at an ultralow concentration by the naked eye in a proof-of-concept application.

Results and Discussion

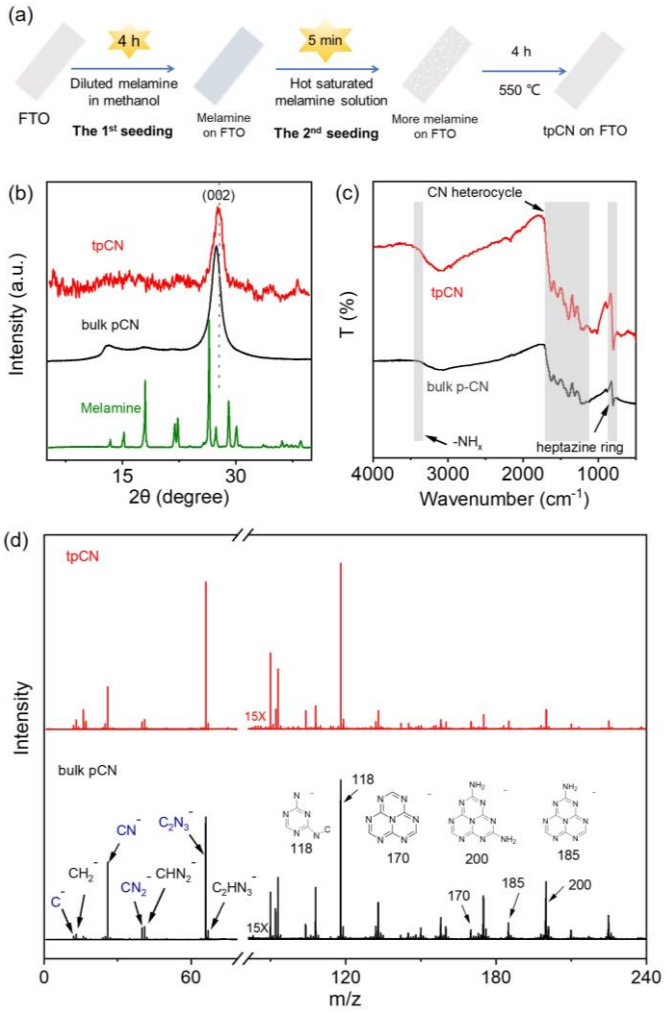

Figure 1. (a) Scheme of the general fabrication procedure for tpCN on the FTO electrode. (b) GIXRD pattern of tpCN on FTO and PXRD patterns of bulk pCN and melamine. (c) FT-IR and (d) TOF-SIMS spectra of tpCN on FTO and bulk pCN.

The general double inoculation and condensation procedures for preparing transparent pCN films (tpCN) are shown in **Figure 1a**. A homogeneous layer of melamine was found to spontaneously seed on FTO in a diluted solution of melamine in methanol (the first seeding), providing the primary interaction with the substrate (see photographs and SEM images in **Figure S1a-c**). To load more melamine precursor on FTO, the seeded FTO glass was further immersed in a hot aqueous solution (97 °C) of saturated melamine for 5 min (the second seeding, see photographs and SEM images in **Figure S1d-f**). The final tpCN films were obtained by calcination of the melamine film at 550 °C for 4 h under N_2 atmosphere. Due to the influence of external environment on the inoculation of melamine on FTO, the calculated film thickness was 342 ± 56 nm (**Figure S2**). Thicker films could be obtained up to 56 μm by increasing the second immersion time in a hot saturated melamine solution (**Figure S3**), but the film became rougher and non-transparent. Notably, when the first seeding time was short (e.g., 5 min), the melamine layer that crystallized on the bare FTO was less crystallized and homogeneous (**Figure. S4**), indicating the first seeding step was slow and required more time to complete.

The crystalline structure of the tpCN layer on the FTO electrode was investigated by grazing incidence X-ray diffraction (GIXRD, **Figure 1b**). The GIXRD patten of tpCN basically exhibited a similar profile to the power X-ray diffraction (PXRD) patten of bulk pCN, demonstrating a sharp, strong interplanar stacking (002) peak at 27.8º, indicative of a layered structure.[12a, 26] The chemical structures of the tpCN films were investigated by Fourier transform infrared spectroscopy (FTIR). Consistent with bulk pCN, the typical stretching modes of -C-N- heterocycles at 1100–1700 cm^{-1} and the sharp peak at 810 cm^{-1} corresponding to heptazine or triazine ring out-of-plane bending were also observed for tpCN (**Figure 1c**).[27] The bonding information was further confirmed by X-ray photoelectron spectroscopy (XPS) spectrum (**Figure S5**). The high-resolution C1s XPS spectrum of tpCN exhibited two typical peaks at 284.6 eV (C2) and 288.3 eV (C1),[28] which were attributed to adventitious carbon and C–N=C coordination, respectively (**Figure S5a**).[29] In the N1s XPS spectrum (**Figure S5b**), four main peaks at 398.4 eV (N1), 399.9 eV (N2), 400.9 eV (N3) and 404.1 eV (N4), corresponding to C-N=C, N-(C)3, C-NH and charge effect, respectively, were observed, which were almost identical to those of bulk pCN.[30] Energy-dispersive spectroscopy (EDS) elemental mapping (**Figure S6**) showed a homogeneous distribution of C and N within the tpCN layer at a C/N atomic ratio of 0.69, which was close to that of bulk pCN (0.60) (**Table S1**).

To further verify the detailed heptazine or triazine subunit, time-of-flight secondary ion mass spectra (TOF-SIMS) of tpCN and bulk pCN were measured (**Figure 1d**), showing a highly homogeneous distribution of carbon nitride-related species. In the fingerprint region, the fragments at m/z 12, 26, 40, 42, and 66 can be assigned to C^-, CN^-, CN_2^-, CNO^-, and C_2N_3 groups,[31] respectively, implying the repeating C–N unit backbone of the tpCN film. More interestingly, in the high m/z region, a clear periodic signal indicated that a highly ordered version of the typical heptazine molecular structure was observed for tpCN, consistent with bulk pCN.[32] Matrix-free laser desorption/ionization time-of-flight (LDI-TOF) mass spectrometry (**Figure S7**) also

supported the heptazine subunit in tpCN.[25, 33]It should be noted that the maintenance of the same heptazine-based molecular structure as pCN on the electrode was essential for realizing the higher orbital delocalization and the higher ECL efficiency for pCN, but often challenged by direct thermal condensation of carbon nitride monomer on the substrate electrode,[34] owing to variations in growth conditions between FTO substrates and the standard crucibles.[28a, 35] It was assumed that the first pre-seed layer provided a buffer to minimize the interfacial differences. Although techniques such as FT-IR and XPS were often used to identify the structure of pCN films, few convincible evidences, such as mass spectroscopy, were given to unambiguously verify the same molecular structure as that in conventional bulk pCN.

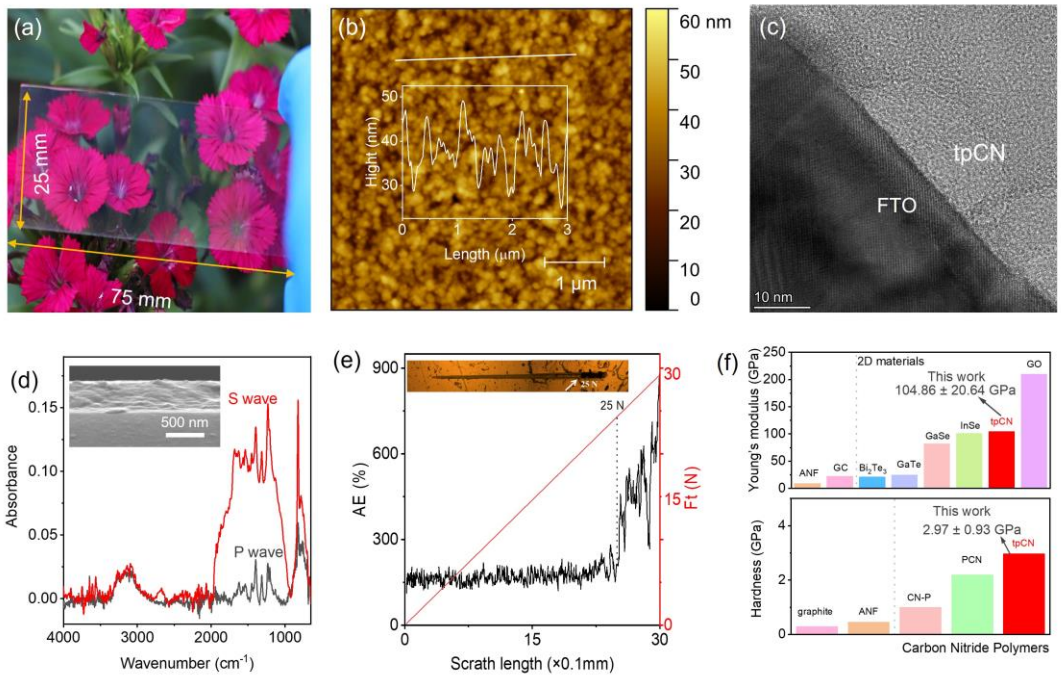

Figure 2. (a) Photograph of tpCN on FTO in front of the flowers. (b) AFM image of tpCN on FTO. Inset: corresponding height profile of a straight white line. (c) HR-TEM image of the tpCN electrode cross-section. (d) Polarized FTIR spectra of tpCN on FTO using s-polarized (S-wave) and p-polarized (P-wave) light. Inset: SEM image of the cross-section showing layers. (e) Scratch adhesion curve of the AE signal. Inset: scratch morphology of tpCN. (f) Comparison of Young's modulus and hardness of the tpCN film with other typical 2D materials, nanocarbon, and carbon nitrides in the literature.

Transparent tpCN on FTO (**Figure 2a**) was qualitatively evaluated using a UV-vis absorption curve (**Figure S8a**). The typical sharp absorption edge of semiconductors was observed for both tpCN and bulk CN, but the former had a much lower baseline, indicating higher transparency in the visible range (**Figure S8b**).[36] The surface topography of the tpCN films was characterized using atomic force microscopy (AFM, **Figure 2b**). The surface of tpCN was smooth and homogeneous, with a fluctuating height of only ca. 20 nm, distinct from those of non-transparent carbon nitride films consisting of much larger particle aggregations (**Figure S9**). The high-resolution TEM

(HR-TEM) image of the cross-section (**Figure 2c**), which was obtained using a focused ion beam (FIB, **Figure S10**), further disclosed that the carbon nitride film and FTO were in close contact at the nanoscale, showing the crucial function of careful pre-seeding in the film preparation (see the control samples in **Figure S2**).

The molecular orientation of the tpCN layer on FTO was examined using IR dichroism. As shown in **Figure 2d**, the peaks at approximately 810 and 1100-1700 cm^{-1}, typically attributed to out-of-plane bending of the triazine or heptazine ring, and the C-N heterocycle stretching vibrations increased when s-polarized light (S wave) was applied with respect to p-polarized light (P wave).[37] This suggested that the π-planes in the tpCN film were highly oriented in a direction parallel to the substrate surface, which is consistent with the observation of the layered texture of tpCN on FTO from the cross-sectional SEM image (**Figure 2d, inset**).[34] In this sense, tpCN not only showed excellent overall uniformity but also had an internal molecular orientation, which was supposed to have a significant influence on the mechanical properties. In general, excellent mechanical properties are essential for practical applications in long-term operations, particularly under external impacts or vibrations from the environment.

Interestingly, apart from transparency, tpCN with a graphitic structure also exhibited exceptional mechanical properties, which have been rarely explored in previous studies with respect to β-phased carbon nitrides. The cohesive strength and interfacial adhesion strength of the films were studied in terms of critical loads by scratch testing. The adhesion strength was defined as the load corresponding to the complete and continuous delamination events with a large-area exposure of the substrate.[38] **Figure 2e** shows the adhesion strength of the films and their scratch-track morphologies. The first intense acoustic emission peak was observed at a load of approximately 25 N, which was ascribed to the first critical failure of the film from the FTO. This value was confirmed by optical micrograph analysis,[39] where adhesive failure was clearly observed. As the number of cycles increased to three, the substrate was exposed to approximately the same 25 N,[40] much higher than the spin-coated carbon nitride film by a factor of five, suggesting that tpCN strongly adhered to the FTO substrate against intense scrape from external forces. A maximum load of 623.82 μN was used for the nanoindentation tests. At least 10 nanoindentation tests were performed at various sites across each film surface to determine their mechanical properties (**Figure S11a**). The resultant hardness (H) and elastic modulus (E) of tpCN were 2.97 and 104.86 GPa (**Figure S11b-c**), respectively, indicative of a typical hard film. It is worth noting that these values were higher than those of all previously reported carbon nitride films,[37, 41] graphite,[41a] glassy carbon (GC),[42] several 2D materials,[43] and other hard polymer materials such as polyimide and Kevlar thin films (**Figure 2f**).[42, 44] Despite being less than graphene,[45] graphene derivatives, and diamond films, [46] for a polymer film condensed at only 550 °C, the mechanical properties are already very impressive, that is, the tpCN electrode not only possesses outstanding transparency but also offers unexpected mechanical protection against damage, such as external impacts or vibrations from the environment.

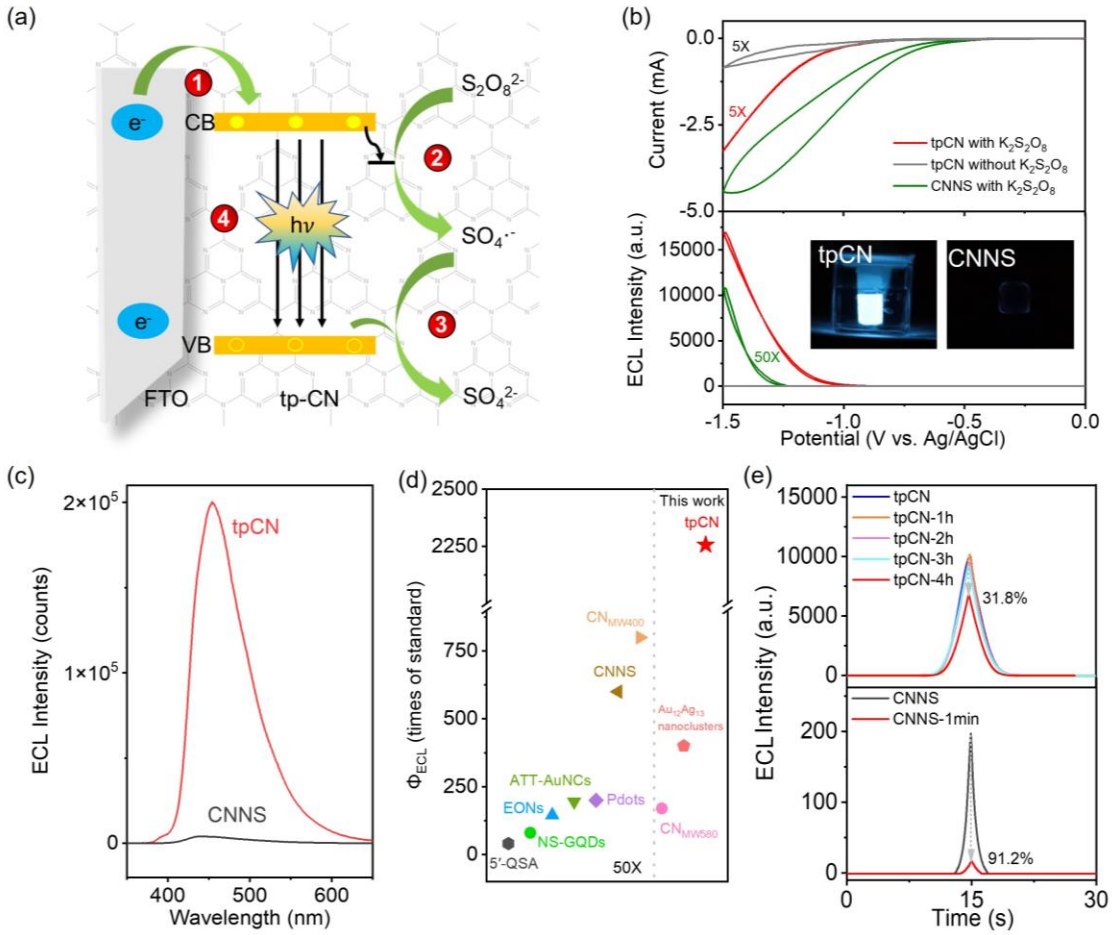

Figure 3. (a) Proposed cathodic ECL mechanism for carbon nitrides. (b) CV and ECL curves of tpCN and CNNS. Inset: Photographs of tpCN and CNNS electrodes under applied voltage. (c) Wavelength-resolved ECL spectrum of tpCN and CNNS under -1.5 V vs. Ag/AgCl that was used for calculating the total number of photons. Electrolytes:0.01 M PBS, 0.1 M KCl, and 25 mM $K_2S_2O_8$. (d) ECL efficiency comparison of tpCN and other counterparts in previous reports. (e) ECL intensities of the tpCN and CNNS electrodes after different sonication time in a cleaner bath (400 W).

ECL refers to luminescence produced by chemical reactions triggered by externally applied potentials. **Figure 3a** shows the four general processes of cathodic ECL at carbon nitride electrodes using $K_2S_2O_8$ as the co-reactant (**Eq. S1-5**).[23, 25, 47] First, electrons were injected from FTO into the conduction band (CB) of carbon nitrides (**Eq. S1**). Next, co-reactant $K_2S_2O_8$ was reduced by excited electrons, thus generating $SO_4^{\bullet-}$ (**Eq. S2**). The third step involved the production of holes in the valence band (VB) by generated $SO_4^{\bullet-}$ (**Eq. S3-4**).[13a] Finally, the electrons in the CB and holes in the VB recombine with the emission of light (**Eq. S5**). The cyclic voltammogram (CV)-ECL curves in **Figure 3b** showed that the electrochemical reduction and ECL generation of tpCN were almost simultaneously occurred at ca. -1.0 V. The control CV curves without $K_2S_2O_8$ showed only a nominal current and ECL, indicating negligible polarization of water during the reduction of $K_2S_2O_8$. Notably, with $K_2S_2O_8$, the CV curve was

incomplete. This is typically attributed to the high iR drop of tpCN, which causes the reduction wave to exceed the electrochemical window.[25] No obvious observation of the electrochemical reduction peak of $K_2S_2O_8$ indicated that the coating of tpCN on FTO was dense and pinhole-free. In contrast, the electrochemical reduction and ECL at the CNNS electrode with $K_2S_2O_8$ occurred at ca. -0.5 V and -1.2 V, respectively. This indicates that the early $K_2S_2O_8$ reduction occurred most presumably at pinholes at a lower overpotential, but this was not sufficient to inject electrons into the CB of the carbon nitrides. As such, the electrons consumed by $K_2S_2O_8$ reduction at the tpCN electrode were supplied only from the tpCN layer rather than from FTO, which would make more use of electrons in ECL and lead to a higher ECL efficiency.

Interestingly, the ECL intensity at tpCN collected by a photomultiplier tube (PMT), regardless of wavelength, was much larger than that at CNNS (**Figure 3b**), and the ECL emission could be easily observed with the naked eye (**Figure 3b inset**). For fair comparison, the intrinsic ECL efficiency of the tpCN photoelectrode was further evaluated by considering the number of generated photons and consumed electrons (**Eq. 1**):[48]

$$\Phi_{ECL}=\frac{\left(\frac{\int ECL\,dt}{\int Currentdt}\right)x}{\left(\frac{\int ECLdt}{\int Currentdt}\right)st}\times 100\% \qquad (1)$$

where "ECL" and "Current" represent integrated ECL photon numbers from the corrected ECL spectrum according to the count sensitivity of PMT at different light wavelengths and Faradaic electrochemical current values, respectively; "st" refers to the $Ru(bpy)_3Cl_2/K_2S_2O_8$ standard; and "x" refers to different carbon nitride electrodes. The potential was fixed at -1.5 V vs. Ag/AgCl by chronoamperometry in 0.01 M PBS (pH 7.4) containing 25 mM $K_2S_2O_8$ and 0.1 M KCl. More details on the ECL efficiency determination are described in the experimental procedures in the Supporting Information. As a result, the cathodic Φ_{ECL} for tpCN was 132 times higher than that of CNNS synthesized from the same precursor, reaching 2256 times that of the reference $Ru(bpy)_3Cl_2/K_2S_2O_8$ system, which is a new record for metal-free ECL emitters (**Figure 3d**, **Table S2**).

Furthermore, owing to its superior mechanical properties (**Figure 2e, f**), the tpCN electrode demonstrated excellent stability in ECL owing to external impacts or vibrations from the environment. ECL stability measurements showed that the original ECL intensity of tpCN still remained unchanged in the first 3 h of sonication, whereas 1 min of sonication resulted in a significant decrease of ca. 91.2% in ECL intensity (**Figure 3e**). The SEM images demonstrated that the tpCN film on FTO remained almost intact under sonication, but the control CNNS film on FTO almost completely peeled off after 1 min of sonication (**Figure S12**). Therefore, the tpCN electrode not only demonstrated exceptionally high ECL efficiency but also outstanding ECL stability, both of which are envisioned for ECL biosensors with high performance in practical applications.

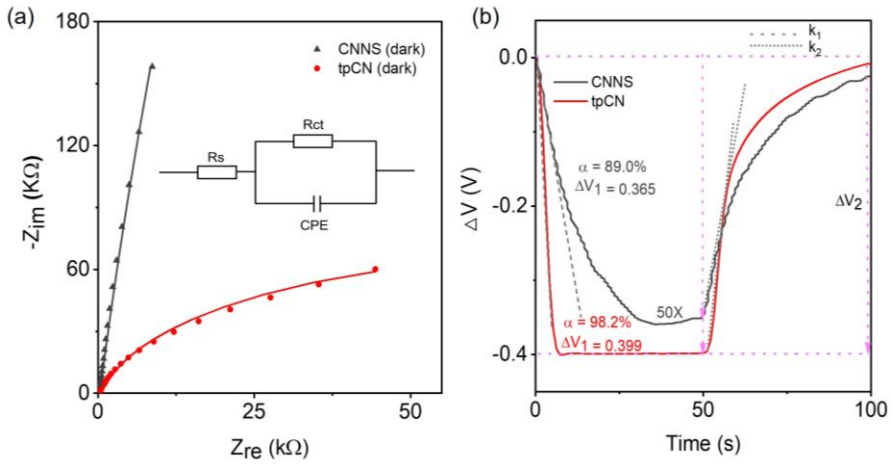

Figure 4. (a) Nyquist plots of tpCN and CNNS in 0.1 M KCl. (b) Open circuit potential of tpCN and CNNS under chopped visible light irradiation in 0.1 M KCl.

To understand the mechanism of the exceptionally high cathode ECL efficiency, the solid-solid interface of carbon nitrides/FTO was explored. In the first set of experiments, the intrinsic charge transfer between carbon nitrides and FTO was investigated by measuring the electrochemical impedance spectrum (EIS) in 0.1 M KCl (**Figure 4a**).[49] The fitting results showed that the charge transfer resistance (R_{ct}) of tpCN/FTO was approximately 200 times smaller than that of CNNS/FTO, which indicated a much higher conductivity, beneficial to a more efficient ECL. As the larger reduction current and lower ECL intensity were inconsistent at the CNNS electrode, the possible pinholes on the tpCN electrode were also examined by EIS measurements using $Fe(CN)_6^{3-}$/$Fe(CN)_6^{4-}$ as electrochemical probes. The Nyquist plots in **Figure S13** verified that the R_{ct} of the CNNS electrode was approximately 1200-fold smaller than that of the tpCN electrode. In this sense, a loose contact between CNNS and FTO could be supposed, which led to a significant reduction in the number of $S_2O_8^{2-}$ be futilely reduced at FTO pinholes, since the reduction of CNNS occurred at a more negative potential (**Figures S14**). To further support this assumption, the charges consumed by the Faraday process, including $K_2S_2O_8$ and tpCN reduction in ECL, were quantitatively assessed by subtracting the consumed charge in chronoamperometric measurements without $K_2S_2O_8$ from that with $K_2S_2O_8$ (see further discussion in **Figure S15a, b**). As expected, the charge consumed during the Faraday process of the CNNS electrode was greater than that of the tpCN electrode (**Figure S15c**) by a factor of 3. Therefore, the tpCN layer on the FTO had fewer pinholes and was more compact than the most commonly used CNNS in previous studies, which favored the use of electrons.

The photon dynamics of ECL for tpCN and CNNS were studied using open-circuit photovoltage (OCP) measurements under chopped light (**Figure 4b**). The OCP of tpCN increased with time under irradiation and gradually reached a plateau. In contrast, the slope (k_1) of tpCN was higher than that of CNNS,[50] indicating faster electrochemical excitation kinetics,[51] which was consistent with the more positive ECL onset potential (**Figure 3b**). Notably, a similar trend was observed for the stable OCP (ΔV_1) under irradiation for both tpCN and CNNS, but the former was approximately 55 times higher.

This indicated that tpCN had higher excited-electron storage capability.[52] In addition, the corresponding slope during light-off was an indicator of electron-hole recombination kinetics (k_2), which was also higher in tpCN than in CNNS by a factor of 91. The surface deep electron-trapping state can be evaluated by the ratio of $\Delta V_2/\Delta V_1$ (α). The ΔV_1, ΔV_2, k_1, and k_2 values of tpCN and CNNS were summarized in **Table S3**. It was found that α of tpCN was closer to 1, while α of CNNS was 0.89, suggesting that tpCN had much less surface deep electron trapping.[25] Therefore, the OCP measurements revealed that tpCN had a higher excited electron-storage capacity, more favorable excitation, faster electron-hole recombination kinetics, and fewer surface deep trapping states of electrons than CNNS. All these factors are beneficial for a high ECL intensity. As such, further considering the fact that fewer electrons are consumed, an increased ECL efficiency would be obtained by tpCN, according to **Eq. 1**.

In this regard, the significantly improved ECL efficiencies for tpCN were the result of several factors. (1) The high-quality pin-hole free film minimized futile co-reagent reduction, thus improving the usage efficiency of electrons. (2) Compared to ill condensation, the maintenance of the higher orbital delocalized heptazine subunit was the same as that in bulk pCN and improved the ECL kinetics, including higher conductivity, higher excited electron-storage capacity, more favorable excitation, faster electron-hole recombination kinetics, and less surface deep trapping state of electrons. They promoted excitation-state generation and subsequent light emission. (3) The transparent film suppressed the self-absorption of the photons produced by the ECL. It was assumed that the first spontaneous seeding in sufficient time, which provided the primary interaction with the substrate in preparation, played a central role.

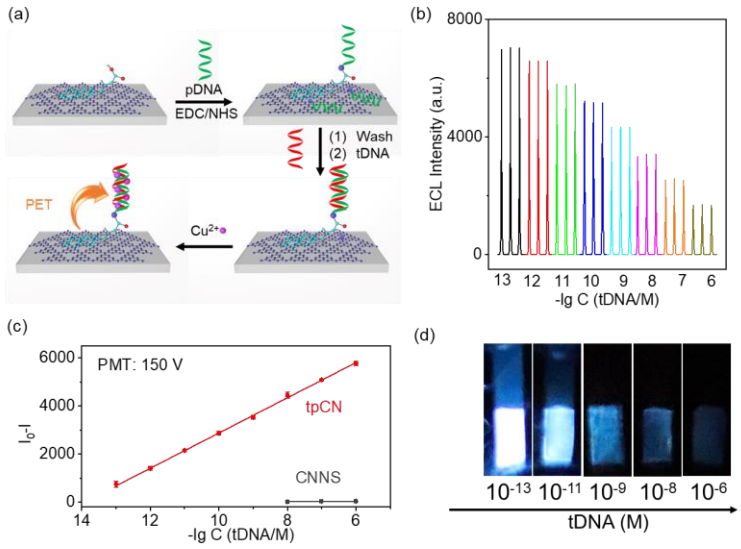

Figure 5. (a) Scheme of the general procedure for a tpCN-based ECL biosensor for DNA detection. (b) ECL response of tpCN upon the addition of 10^{-13}–10^{-6} M tDNA. (c) Calibration curves of DNA biosensing using tpCN and CNNS as ECL probes, respectively. (d) Photographs of ECL at tpCN electrode in solution containing different concentrations of tDNA.

pCNIt is highly envisioned that the newly recorded ECL efficiency would greatly boost the sensitivity of biosensing. As a proof-of-concept application, a well-developed DNA probe was selected as a model biomolecule to conjugate to the tpCN surface using Py-COOH (sodium salt) as the covalent linker.[47a] Based on the principle of complementary base pairing, target ssDNA (tDNA) can be captured to form a tDNA-pDNA hybrid (**Figure 5a**). Notably, the ECL intensity of tpCN was not affected by dissolved oxygen in the electrolyte (**Figure S16a**). The ECL of tpCN was stable under continuous cyclic voltammetry scans (**Figure S16b**), which is a prerequisite for ECL biosensors. Because Cu^{2+} can bind to the N 7 position of the DNA base to form a DNA-Cu^{2+} complex,[53] the amount of Cu^{2+} adsorbed on DNA was proportional to the total amount of DNA. **Figure 5b** shows that ECL intensity decreased with increasing tDNA concentration. As a control, a similar ECL sensor using a dispersion containing Py-COOH (sodium salt)-modified CNNS was constructed. It was noted that under a low biased potential (150 V) for the photomultiplier tube (PMT), the logarithmic value of the ECL intensity at the tpCN electrode scaled linearly with the concentration of tDNA from 10^{-6} to 10^{-13} M, with a very low detection limit of 2.7×10^{-14} M (S/N = 3). This was superior to that of the conventional CNNS under the same conditions (**Figure 5c**). The excellent performance of the tpCN-based ECL biosensor has made it one of the most sensitive signal-amplification-free biosensors for DNA. Moreover, because of the new record of cathodic ECL efficiency, it could be further developed into the brightest visual cathodic ECL biosensor by the naked eye for DNA detection with uncompromising performance (**Figure 5d**).

Conclusion

In summary, we reported the direct synthesis of high-quality carbon nitride thin films by double inoculation on substrates and *in situ* thermal condensation. Interestingly, owing to the intimate contact of carbon nitride with the substrates at the nanoscale and oriented growth in a direction parallel to the substrate, the optimized tpCN was transparent and exhibited the strongest Young's modulus (104.86 GPa)/hardness (2.90 GPa) among the graphitic carbon nitride family, which was superior to typical hard polymer materials. Moreover, tpCN demonstrated the highest cathodic ECL efficiency thus far (2256 times that of the $Ru(bpy)_3Cl_2/K_2S_2O_8$ reference) among metal-free ECL emitters. Mechanism studies showed that the significantly improved ECL efficiencies for tpCN were ascribed to few pinholes suppressing futile co-reagent reduction, maintenance of more orbit-delocalized heptazine subunits improving the ECL kinetics, and transparent film avoiding self-absorption of ECL. It was assumed that double inoculation, which provided the primary interaction of carbon nitride with the substrate and the succedent growth, played a crucial role in preparation. As a proof-of-concept application of tpCN with exceptionally high ECL efficiency, a visual biosensor using the naked eye was demonstrated with a linear detection range of 10^{-6} to 10^{-13} M, one of the most sensitive signal-amplification-free biosensors for DNA. This work provides a facile way to prepare tpCNs with high ECL efficiency for broader applications, such as visual bioassays and cell imaging.

Reference

[1] a) A. Zanut, A. Fiorani, S. Canola, T. Saito, N. Ziebart, S. Rapino, S. Rebeccani, A. Barbon, T. Irie, H.-P. Josel, F. Negri, M. Marcaccio, M. Windfuhr, K. Imai, G. Valenti, F. Paolucci, *Nat. Commun.* **2020**, *11*, 2668; b) S. Voci, B. Goudeau, G. Valenti, A. Lesch, M. Jović, S. Rapino, F. Paolucci, S. Arbault, N. Sojic, *J. Am. Chem. Soc.* **2018**, *140*, 14753-14760; c) J. Zhang, R. Jin, D. Jiang, H.-Y. Chen, *J. Am. Chem. Soc.* **2019**, *141*, 10294-10299; d) Z. Cao, Y. Shu, H. Qin, B. Su, X. Peng, *ACS Cent. Sci.* **2020**, *6*, 1129-1137; e) Y.-J. Li, W.-R. Cui, Q.-Q. Jiang, Q. Wu, R.-P. Liang, Q.-X. Luo, J.-D. Qiu, *Nat. Commun.* **2021**, *12*; f) D. Pan, Z. Fang, E. Yang, Z. Ning, Q. Zhou, K. Chen, Y. Zheng, Y. Zhang, Y. Shen, *Angew. Chem. Int. Ed.* **2020**, *59*, 16747-16754; g) A. Chen, W. Liang, H. Wang, Y. Zhuo, Y. Chai, R. Yuan, *Anal. Chem.* **2019**, *92*, 1379-1385; h) R. Luo, H. Lv, Q. Liao, N. Wang, J. Yang, Y. Li, K. Xi, X. Wu, H. Ju, J. Lei, *Nat. Commun.* **2021**, *12*; i) J. I. Lee, H. Choi, S. H. Kong, S. Park, D. Park, J. S. Kim, S. H. Kwon, J. Kim, S. H. Choi, S. G. Lee, D. H. Kim, M. S. Kang, *Adv. Mater.* **2021**, *33*, 2100321; j) H. Zhu, R. Jin, Y. C. Chang, J. J. Zhu, D. Jiang, Y. Lin, W. Zhu, *Adv. Mater.* **2021**, *33*, 2105039; k) X. Zhou, D. Zhu, Y. Liao, W. Liu, H. Liu, Z. Ma, D. Xing, *Nat. Protoc.* **2014**, *9*, 1146-1159.

[2] a) I. Rubinstein, A. J. Bard, *J. Am. Chem. Soc.* **2002**, *103*, 512-516; b) C. Ma, Y. Cao, X. Gou, J.-J. Zhu, *Anal. Chem.* **2019**, *92*, 431-454.

[3] a) N. Wang, H. Gao, Y. Li, G. Li, W. Chen, Z. Jin, J. Lei, Q. Wei, H. Ju, *Angew. Chem. Int. Ed.* **2020**, *60*, 197-201; b) K. N. Swanick, S. Ladouceur, E. Zysman-Colman, Z. Ding, *Angew. Chem. Int. Ed.* **2012**, *124*, 11241-11244.

[4] a) C. Booker, X. Wang, S. Haroun, J. Zhou, M. Jennings, B. L. Pagenkopf, Z. Ding, *Angew. Chem. Int. Ed.* **2008**, *47*, 7731-7735; b) J.-W. Oh, Y. O. Lee, T. H. Kim, K. C. Ko, J. Y. Lee, H. Kim, J. S. Kim, *Angew. Chem. Int. Ed.* **2009**, *48*, 2427-2427.

[5] a) S. Carrara, A. Aliprandi, C. F. Hogan, L. De Cola, *J. Am. Chem. Soc.* **2017**, *139*, 14605-14610; b) X. Wei, M. J. Zhu, Z. Cheng, M. Lee, H. Yan, C. Lu, J. J. Xu, *Angew. Chem. Int. Ed.* **2019**, *131*, 3194-3198; c) H. Peng, Z. Huang, H. Deng, W. Wu, K. Huang, Z. Li, W. Chen, J. Liu, *Angew. Chem. Int. Ed.* **2019**, *59*, 9982-9985.

[6] H. Liang, D. Song, J. Gong, *Biosens. Bioelectron.* **2014**, *53*, 363-369.

[7] a) H. Peng, Z. Huang, Y. Sheng, X. Zhang, H. Deng, W. Chen, J. Liu, *Angew. Chem. Int. Ed.* **2019**, *131*, 11817-11820; b) L. Yang, B. Zhang, L. Fu, K. Fu, G. Zou, *Angew. Chem. Int. Ed.* **2019**, *58*, 6901-6905.

[8] N. Wang, Z. Wang, L. Chen, W. Chen, Y. Quan, Y. Cheng, H. Ju, *Chem. Sci.* **2019**, *10*, 6815-6820.

[9] a) J. I. Kim, I.-S. Shin, H. Kim, J.-K. Lee, *J. Am. Chem. Soc.* **2005**, *127*, 1614-1615; b) M. A. Haghighatbin, S. E. Laird, C. F. Hogan, *Curr Opin Electrochem.* **2018**, *7*, 216-223.

[10] Y. Zheng, H. Yang, L. Zhao, Y. Bai, X. Chen, K. Wu, S. Liu, Y. Shen, Y. Zhang, *Anal. Chem.* **2022**, *94*, 3296-3302.

[11] a) R. Ishimatsu, S. Matsunami, T. Kasahara, J. Mizuno, T. Edura, C. Adachi, K. Nakano, T. Imato, *Angew. Chem. Int. Ed.* **2014**, *126*, 7113-7116; b) S. Chen, H. Ma, J. W. Padelford, W. Qinchen, W. Yu, S. Wang, M. Zhu, G. Wang, *J. Am. Chem. Soc.* **2019**, *141*, 9603-9609.

[12] a) X. Wang, K. Maeda, A. Thomas, K. Takanabe, G. Xin, J. M. Carlsson, K. Domen, M. Antonietti, *Nat. Mater.* **2008**, *8*, 76-80; b) I. Ghosh, J. Khamrai, A. Savateev, N. Shlapakov, M. Antonietti, B. König, *Science.* **2019**, *365*, 360-366; c) D. Zhao, Y. Wang, C.-L. Dong, Y.-C. Huang, J. Chen, F. Xue, S. Shen, L. Guo, *Nat. Energy.* **2021**, *6*, 388-397; d) Z. Teng, Q. Zhang, H. Yang, K. Kato, W. Yang, Y.-R. Lu, S. Liu, C. Wang, A. Yamakata, C. Su, B. Liu, T. Ohno, *Nat. Catal.* **2021**, *4*, 374-

384; e) M. Volokh, G. Peng, J. Barrio, M. Shalom, *Angew. Chem. Int. Ed.* **2019**, *58*, 6138-6151; f) R. Kuriki, K. Sekizawa, O. Ishitani, K. Maeda, *Angew. Chem. Int. Ed.* **2015**, *54*, 2406-2409; g) W.-J. Ong, L.-L. Tan, Y. H. Ng, S.-T. Yong, S.-P. Chai, *Chem. Rev.* **2016**, *116*, 7159-7329; h) H. Schlomberg, J. Kröger, G. Savasci, M. W. Terban, S. Bette, I. Moudrakovski, V. Duppel, F. Podjaski, R. Siegel, J. Senker, R. E. Dinnebier, C. Ochsenfeld, B. V. Lotsch, *Chem. Mater.* **2019**, *31*, 7478-7486; i) M. Liu, C. Wei, H. Zhuzhang, J. Zhou, Z. Pan, W. Lin, Z. Yu, G. Zhang, X. Wang, *Angew. Chem. Int. Ed.* **2021**, *61*, 202113389-202113394.

[13] a) C. Cheng, Y. Huang, X. Tian, B. Zheng, Y. Li, H. Yuan, D. Xiao, S. Xie, M. M. F. Choi, *Anal. Chem.* **2012**, *84*, 4754-4759; b) L. Chen, D. Huang, S. Ren, T. Dong, Y. Chi, G. Chen, *Nanoscale.* **2013**, *5*, 225-230; c) L. Chen, X. Zeng, P. Si, Y. Chen, Y. Chi, D.-H. Kim, G. Chen, *Anal. Chem.* **2014**, *86*, 4188-4195; d) R. Zou, Y. Lin, C. Lu, *Anal. Chem.* **2021**, *93*, 2678-2686; e) Z. Zhou, Q. Shang, Y. Shen, L. Zhang, Y. Zhang, Y. Lv, Y. Li, S. Liu, Y. Zhang, *Anal. Chem.* **2016**, *88*, 6004-6010.

[14] A. Tashakory, N. Karjule, L. Abisdris, M. Volokh, M. Shalom, *Adv. Sustain.* **2021**, *5*, 2100005.

[15] a) Y. Zhang, M. Antonietti, *Chem Asian J.* **2010**, *5*, 1307; b) S. Lou, Z. Zhou, Y. Shen, Z. Zhan, J. Wang, S. Liu, Y. Zhang, *ACS Appl. Mater.* **2016**, *8*, 22287-22294.

[16] N. Karjule, R. Phatake, M. Volokh, I. Hod, M. Shalom, *Small Methods.* **2019**, *3*, 1900401.

[17] B. Kumru, D. Cruz, T. Heil, B. V. K. J. Schmidt, M. Antonietti, *J. Am. Chem. Soc.* **2018**, *140*, 17532-17537.

[18] a) X. Jiang, H. Wang, Y. Chai, W. Shi, R. Yuan, *Anal. Chem.* **2020**, *92*, 8992-9000; b) X. Jiang, H. Wang, Y. Chai, H. Li, W. Shi, R. Yuan, *Anal. Chem.* **2019**, *91*, 10258-10265; c) Y. Feng, Q. Wang, J. Lei, H. Ju, *Biosens. Bioelectron.* **2015**, *73*, 7-12.

[19] a) J. Bian, C. Huang, R.-Q. Zhang, *ChemSusChem.* **2016**, *9*, 2723-2735; b) C. Jia, L. Yang, Y. Zhang, X. Zhang, K. Xiao, J. Xu, J. Liu, *ACS Appl. Mater.* **2020**, *12*, 53571-53591.

[20] a) J. Bian, Q. Li, C. Huang, J. Li, Y. Guo, M. Zaw, R.-Q. Zhang, *Nano Energy.* **2015**, *15*, 353-361; b) J. Bian, J. Li, S. Kalytchuk, Y. Wang, Q. Li, T. C. Lau, T. A. Niehaus, A. L. Rogach, R.-Q. Zhang, *Chemphyschem.* **2015**, *16*, 954-959.

[21] a) G. Peng, J. Albero, H. Garcia, M. Shalom, *Angew. Chem. Int. Ed.* **2018**, *57*, 15807-15811; b) J. Qin, J. Barrio, G. Peng, J. Tzadikov, L. Abisdris, M. Volokh, M. Shalom, *Nat. Commun.* **2020**, *11*, 4701.

[22] B. Guo, L. Tian, W. Xie, A. Batool, G. Xie, Q. Xiang, S. U. Jan, R. Boddula, J. R. Gong, *Nano Lett.* **2018**, *18*, 5954-5960.

[23] T. Zhao, Q. Zhou, Y. Lv, D. Han, K. Wu, L. Zhao, Y. Shen, S. Liu, Y. Zhang, *Angew. Chem. Int. Ed.* **2019**, *59*, 1139-1143.

[24] M. Volokh, G. Peng, J. Barrio, M. Shalom, *Angew. Chem. Int. Ed.* **2019**, *131*, 6198-6211.

[25] Y. Fang, Y. Hou, H. Yang, R. Chen, W. Li, J. Ma, D. Han, X. Cao, S. Liu, Y. Shen, Y. Zhang, *Adv. Opt. Mater.* **2022**, *10*, 2201017.

[26] a) B. V. Lotsch, M. Döblinger, J. Sehnert, L. Seyfarth, J. Senker, O. Oeckler, W. Schnick, *Chem. Eur. J.* **2007**, *13*, 4969-4980; b) X. Zhang, X. Xie, H. Wang, J. Zhang, B. Pan, Y. Xie, *J. Am. Chem. Soc.* **2012**, *135*, 18-21; c) Z. Zhou, J. Wang, J. Yu, Y. Shen, Y. Li, A. Liu, S. Liu, Y. Zhang, *J. Am. Chem. Soc.* **2015**, *137*, 2179-2182.

[27] M. Shalom, S. Gimenez, F. Schipper, I. Herraiz-Cardona, J. Bisquert, M. Antonietti, *Angew. Chem. Int. Ed.* **2014**, *126*, 3728-3732.

[28] a) A. Thomas, A. Fischer, F. Goettmann, M. Antonietti, J.-O. Müller, R. Schlögl, J. M. Carlsson, *J.*

Mater. Chem. **2008**, *18*, 4893-4908; b) J. Xu, H. Wang, C. Zhang, X. Yang, S. Cao, J. Yu, M. Shalom, *Angew. Chem. Int. Ed.* **2017**, *129*, 8546-8550.

[29] Z. Lin, X. Wang, *Angew. Chem. Int. Ed.* **2013**, *125*, 1779-1782.

[30] L. Chen, R. Yan, M. Oschatz, L. Jiang, M. Antonietti, K. Xiao, *Angew. Chem. Int. Ed.* **2020**, *59*, 9067-9073.

[31] a) Z. Yu, X. Yue, J. Fan, Q. Xiang, *ACS Catal.* **2022**, *12*, 6345-6358; b) G. Wu, S. S. Thind, J. Wen, K. Yan, A. Chen, *Appl. Catal. B.* **2013**, *142-143*, 590-597; c) S. Kang, M. He, M. Chen, J. Wang, L. Zheng, X. Chang, H. Duan, D. Sun, M. Dong, L. Cui, *Carbon.* **2020**, *159*, 51-64.

[32] a) L. Cui, Z. Fang, Y. Liu, M. Chen, C. Yin, J. Wang, Z. Wang, M. Dong, S. Kang, P. Liu, *Inorg. Chem. Front.* **2019**, *6*, 1304-1311; b) Z. Lin, J. Zheng, G. Lin, Z. Tang, X. Yang, Z. Cai, *Anal. Chem.* **2015**, *87*, 8005-8012.

[33] V. W.-h. Lau, M. B. Mesch, V. Duppel, V. Blum, J. Senker, B. V. Lotsch, *J. Am. Chem. Soc.* **2015**, *137*, 1064-1072.

[34] Z. Liu, C. Wang, Z. Zhu, Q. Lou, C. Shen, Y. Chen, J. Sun, Y. Ye, J. Zang, L. Dong, C.-X. Shan, *Matter.* **2021**, *4*, 1625-1638.

[35] a) M. J. Bojdys, J.-O. Müller, M. Antonietti, A. Thomas, *Chem. Eur. J.* **2008**, *14*, 8177-8182; b) X. Xu, Z. Zhang, J. Dong, D. Yi, J. Niu, M. Wu, L. Lin, R. Yin, M. Li, J. Zhou, S. Wang, J. Sun, X. Duan, P. Gao, Y. Jiang, X. Wu, H. Peng, R. S. Ruoff, Z. Liu, D. Yu, E. Wang, F. Ding, K. Liu, *Sci. Bull.* **2017**, *62*, 1074-1080; c) X. Xu, Z. Zhang, L. Qiu, J. Zhuang, L. Zhang, H. Wang, C. Liao, H. Song, R. Qiao, P. Gao, Z. Hu, L. Liao, Z. Liao, D. Yu, E. Wang, F. Ding, H. Peng, K. Liu, *Nat. Nanotechnol.* **2016**, *11*, 930-935.

[36] H. Shi, S. Long, J. Hou, L. Ye, Y. Sun, W. Ni, C. Song, K. Li, G. G. Gurzadyan, X. Guo, *Chem. Eur. J.* **2019**, *25*, 5028-5035.

[37] H. Arazoe, D. Miyajima, K. Akaike, F. Araoka, E. Sato, T. Hikima, M. Kawamoto, T. Aida, *Nat. Mater.* **2016**, *15*, 1084-1089.

[38] a) Z. Yan, H. Zhou, X. Zhang, J. Liu, C. Wang, X. Lu, J. Hao, X. Sui, *Tribol Int.* **2022**, *170*, 107431; b) J. Shuai, X. Zuo, Z. Wang, L. Sun, R. Chen, L. Wang, A. Wang, P. Ke, *J. Mater. Sci. Technol.* **2021**, *80*, 179-190.

[39] a) N. Xu, W. Han, Y. Wang, J. Li, Z. Shan, *Acta Mater.* **2017**, *124*, 343-350; b) R. Akhter, Z. Zhou, Z. Xie, P. Munroe, *Appl. Surf. Sci.* **2021**, *563*, 150356.

[40] R. Wang, H. Liu, Z. Fan, L. Li, Y. Cai, G. Xu, W. Luo, B. Yang, Y. Zhou, Z. Zou, *Nanoscale.* **2018**, *10*, 3342-3349.

[41] a) P. Giusto, D. Cruz, T. Heil, H. Arazoe, P. Lova, T. Aida, D. Comoretto, M. Patrini, M. Antonietti, *Adv. Mater.* **2020**, *32*, 1908140; b) Z. Cai, Z. Song, L. Guo, *ACS Appl. Mater.* **2019**, *11*, 12770-12776.

[42] J. Bauer, A. Schroer, R. Schwaiger, O. Kraft, *Nat. Mater.* **2016**, *15*, 438-443.

[43] a) L. Guo, H. Yan, Q. Moore, M. Buettner, J. Song, L. Li, P. T. Araujo, H.-T. Wang, *Nanoscale.* **2015**, *7*, 11915-11921; b) B. Chitara, A. Ya'akobovitz, *Nanoscale.* **2018**, *10*, 13022-13027; c) Q. Tu, I. Spanopoulos, P. Yasaei, C. C. Stoumpos, M. G. Kanatzidis, G. S. Shekhawat, V. P. Dravid, *ACS Nano.* **2018**, *12*, 10347-10354; d) H. Wang, E. J. Sandoz-Rosado, S. H. Tsang, J. Lin, M. Zhu, G. Mallick, Z. Liu, E. H. T. Teo, *Adv. Funct. Mater.* **2019**, *29*, 1902663; e) Y. Li, C. Yu, Y. Gan, Y. Kong, P. Jiang, D. Zou, P. Li, X. Yu, R. Wu, H. Zhao, C.-F. Gao, J. Li, *Nanotechnology.* **2019**, *30*, 335703; f) J. W. Suk, R. D. Piner, J. An, R. S. Ruoff, *ACS Nano.* **2010**, *4*, 6557-6564.

[44] a) M. Wang, A. E. Emre, J.-Y. Kim, Y. Huang, L. Liu, V. Cecen, Y. Huang, N. A. Kotov, *Nat.*

Commun. **2022**, *13*, 278; b) B. Yang, L. Wang, M. Zhang, J. Luo, Z. Lu, X. Ding, *Adv. Funct. Mater.* **2020**, *30*, 2000186.

[45] Y. Zhang, C. Pan, *Diam Relat Mater.* **2012**, *24*, 1-5.

[46] N. Savvides, T. J. Bell, *Thin Solid Films* **1993**, *228*, 289-292.

[47] a) J. Ji, J. Wen, Y. Shen, Y. Lv, Y. Chen, S. Liu, H. Ma, Y. Zhang, *J. Am. Chem. Soc.* **2017**, *139*, 11698-11701; b) M. M. Richter, *Chem. Rev.* **2004**, *104*, 3003-3036; c) W. Miao, *Chem. Rev.* **2008**, *108*, 2506-2553; d) L. Hu, G. Xu, *Chem. Soc. Rev.* **2010**, *39*, 3275.

[48] M. Hesari, K. N. Swanick, J.-S. Lu, R. Whyte, S. Wang, Z. Ding, *J. Am. Chem. Soc.* **2015**, *137*, 11266-11269.

[49] W. Jiang, Y. Zhao, X. Zong, H. Nie, L. Niu, L. An, D. Qu, X. Wang, Z. Kang, Z. Sun, *Angew. Chem. Int. Ed.* **2021**, *60*, 6124-6129.

[50] W. Che, W. Cheng, T. Yao, F. Tang, W. Liu, H. Su, Y. Huang, Q. Liu, J. Liu, F. Hu, Z. Pan, Z. Sun, S. Wei, *J. Am. Chem. Soc.* **2017**, *139*, 3021-3026.

[51] Q. Ruan, T. Miao, H. Wang, J. Tang, *J. Am. Chem. Soc.* **2020**, *142*, 2795-2802.

[52] V. W.-h. Lau, D. Klose, H. Kasap, F. Podjaski, M.-C. Pignié, E. Reisner, G. Jeschke, B. V. Lotsch, *Angew. Chem. Int. Ed.* **2017**, *56*, 510-514.

[53] a) Y.-G. Gao, M. Sriram, A. H. J. Wang, *Nucleic Acids Res.* **1993**, *21*, 4093-4101; b) M. Noguera, J. Bertran, M. Sodupe, *J. Phys. Chem. A.* **2003**, *108*, 333-341; c) R. Oliva, L. Cavallo, *J. Phys. Chem. B.* **2009**, *113*, 15670-15678.